Construction mode detection for autonomous offshore heavy lift operations

Ye, J.; Reppa, V.; Godjevac, M.; Negenborn, R. R.

DOI
10.1016/j.ssci.2020.104991

Publication date
2021

Document Version
Final published version

Published in
Safety Science

Safety Science 133 (2021) 104991

Contents lists available at ScienceDirect

Safety Science

journal homepage: www.elsevier.com/locate/safety

Construction mode detection for autonomous offshore heavy lift operations☆

J. Ye[a], V. Reppa[a], M. Godjevac[b], R.R. Negenborn[a]

[a] Maritime and Transport Technology, Faculty of Mechanical, Maritime and Materials Engineering, Delft University of Technology, 2628CD, the Netherlands
[b] Allseas, Poortweg 12, 2612PA, the Netherlands

ARTICLE INFO

Keywords:
Interconnected operations
Offshore heavy lift
Mode detection
Autonomy
Crane vessel

ABSTRACT

Offshore platforms and windmills are constructed by assembling huge mechanical structures transported by heavy lift vessels. The construction process comprises two interconnected operations, the dynamic positioning (DP) of the vessel and the lifting of heavy loads. The DP system is commonly designed and tuned for the case that there is no load or for the case that the heavy load is free-hanging (mode 1). During the transition from the free-hanging to the case that the vessel is connected to a heavy load which is mounted to the platform (mode 2), the DP system may not be able to preserve the position stability of the vessel, jeopardizing human and system safety. The goal of this work is to design an intelligent monitoring system for the early detection of the transition between the two construction modes by adopting a nonlinear state estimation approach. Simulation results are used for illustrating the effectiveness of the proposed construction mode detection system.

1. Introduction

The vision of waterborne transport includes autonomous shipping operations aiming at enhancing their sustainability, efficiency and safety. Significant number of research and industrial activity has been witnessed towards the autonomy of cargo vessels, which is classified in several levels (Lloyd's Register et al., 2017). The key factors for increasing the levels of vessels' autonomy are digitilization and automatization. For offshore heavy lift operations however, the level of autonomy is still low. The need for higher levels of autonomy in this kind of operations has been intensified due to the increasing demand of energy to assist the growing economy. In these operations, offshore oil platforms are constructed and installed for exploring and exploiting offshore energy (Sun et al., 2012). Such offshore structures are generally transferred and installed by heavy lift vessels with huge cranes (Ye, 2016; Li et al., 2016). At the same time, the removal of these construction installations has become of paramount importance due to the aging of the oil platforms that can harm the environment (Hendrapati et al., 2017), and due to the decreasing profitability.

During a complete offshore removal of an offshore structure, e.g., a topside of a fixed platform, the load is first lifted from the jacket, and then transferred to the shore or to the barge by a heavy lift vessel. Such assignment mainly comprises two interconnected operations, the dynamic positioning (DP) of the crane vessel and the lifting of the heavy load. The lifting of the load is time-consuming and can take up to half an hour (Flint and Stephens, 2008). When the crane is lifting up the load from the shore or the platform, the vessel should remain in the desired position. The interconnection between the vessel dynamics and the crane-load interaction stems from the fact that the lifting of the load can affect the stability of the vessel position and vice versa. Thus, a series of safety–critical tasks during these operations should be carried out meticulously. Among the safety–critical tasks is the transition between two modes of construction: During construction mode 1, the load is lifted by the wires, and is suspended in the air. During construction mode 2, a hydraulic winch on the crane is used to lift the load up using wires. In both modes, the vessel's position is under DP control. In current practice, the DP of the crane vessel is realized using a software-based controller. Studies have shown that instability can be caused during the switching of construction mode if the gains of the DP system are not properly modified on time (Ye, 2016; Flint and Stephens, 2008; Fonteyn, 2015; Bakker, 2015; Harmsen et al., 2018). Particularly, the gains of the DP controller are tuned for the vessel without load, and cannot guarantee stability when there is a sudden change in the vessel-load dynamics (de Jong, 2018; Ye et al., 2017; Waals, 2010; Jenssen, 2008; Sun et al., 2015; Qian et al., 2017; Messineo and Serrani, 2009; Skaare and Egeland, 2006; McKenna and Leithead, 2007). Thus it is essential to switch between these two controllers fast. Note that the switching can be from mode 1 to mode 2 or vice versa depending on the type of construction.

The detection of the switching between the construction modes is

☆ This work is financially supported by the program of China Scholarship Council (CSC) with project No. 201607720003.

https://doi.org/10.1016/j.ssci.2020.104991
Received 21 December 2019; Received in revised form 17 July 2020; Accepted 31 August 2020

not trivial and nowadays is carried out by crane operators on board who transmit this information via oral communication to DP operators who are responsible to switch manually the DP controllers. This detection method relies on the human observation and human decision, which may involve human errors or may be delayed since it is made in hazardous working environment. According to previous studies, human errors play an important role in such offshore accidents (Khan et al., 2006). During the period of 2001–2011, more than 23 collisions have been reported between vessels and offshore facilities on the Norwegian continental shelf, and most of these accidents happened due to wrong decisions (Sandhåland et al., 2015). For underwater constructions, where the load is placed in the sea, unmanned underwater vehicles are used to support the detection of the construction mode, increasing the construction cost. The use of a digital monitoring system to detect the construction mode would assist the operators with decision making, and increase reliability during construction under hazardous environment. Such system can improve safety of offshore heavy lifting, decrease the risk level of such operations during hazardous environment, and paves the way for higher level of autonomy with less manned operation on board.

The detection of the switching between the two construction modes is a binary decision-making problem. Similar decision-making problems can be met in the field of sensor fault detection of nonlinear systems (Reppa et al., 2017; Reppa et al., 2018), onshore transportation to detect the stop or driving mode of automobiles (Lari and Golroo, 2015; Ghorpade et al., 2015; Wu et al., 2016; Shafique and Hato, 2016), or in the field of structural dynamics to detect if a structure is damaged or not (Hou et al., 2018). The detection problem is also the first step for diagnosing faults in a system (De Angelo et al., 2009; Li et al., 2017). There are two main approaches for designing a detection system: (i) using measured input and output signals in combination with a mathematical model, describing the behavior of the system (model-based), (ii) using the measured output signals only (model-free or signal-based or data-driven) (Gao et al., 2015; Blanke et al., 2016; Isermann, 2006). While the design of model-based methods may be more complex compared to the design of model-free methods, they do not necessitate a considerable amount of data to perform detection.

Such detection systems have been developed and applied to guarantee the safety of operation in constructions of offshore wind farms (Badihi et al., 2017; Echavarria et al., 2008; Cho et al., 2018), in oil and gas production (Mishra and Saraf, 2019; Natarajan and Srinivasan, 2010), as well as in dredging, pipe laying and crane operations (Tang and Wang, 2008; Fu et al., 2010; Shuguang et al., 2014). No monitoring system has been developed for the automatic detection of the switching between the offshore heavy lift construction modes yet.

The goal and the main contribution of this work is to improve safety and to lift the autonomy level during offshore heavy lifting by designing a model-based monitoring system for detecting the switching of the construction mode during the removal of the facilities. This monitoring system is an essential part of the digitilization and automatization of the offshore heavy lift operations, where online input and sensor data is used in combination with analytical redundancy (i.e., models) to obtain decisions without the need of human intervention. The main components of the detection system are: (i) an observer-based residual generator, (ii) an adaptive threshold generator, and (iii) detection decision logic (Chen and Patton, 1999; Reppa et al., 2015; Reppa et al., 2016). These components have been designed based on a 6 degrees-of-freedom (DoF) dynamics model of a crane vessel and assuming that the load is in construction mode 2 (i.e., the global position of the load is constant and known), and that the environmental disturbances and the measurement noise are bounded. The inputs of the detection system are the measured position and velocity of crane vessel and the measured tension force acting on the crane wires (as shown in Fig. 1). The output of the detection system is binary, viz. 0 when construction mode 2 is active and 1 otherwise.

The main contributions of this work are:

- The modelling of the 6 DoF dynamics of the crane vessel and the 3 DoF dynamics of the load lifted by the crane wires as two interconnected systems in the state space framework.
- The design of a nonlinear observer based on the dynamics of the crane vessel taking into account only the dynamics of the load in mode 1 that affect the crane vessel due to the interconnection.
- The rigorous and systematic design of adaptive thresholds for decision making.

The added value of the proposed monitoring system is that it can be implemented in the computer used for the DP controller and does not depend on the characteristics of the load or the wires. The proposed scheme is a general solution for mode detection of heavy lift operations, and can be easily adapted to other heavy lift vessels by changing the design parameters. Furthermore, the proposed system provides a fast and reliable way to detect the mode change during the operation.

The impact of using the proposed monitoring system in offshore heavy lift operations is twofold. First, it can increase the level of autonomy by replacing human decision about the switching of the construction mode with the automatic decision of a digital system. Thus less human operators are exposed to hazardous offshore environment. Second, the proposed method can assist the DP system and crane controller on board, and can improve the performance of the DP system with fast detection of mode switch, leading to a safer and more stable vessel position during offshore heavy lift.

The paper is organized as follows: In Section 2, the modelling of the heavy lift construction modes is described, along with the mathematical models of the crane vessel and the lifted load by the wires. Section 3 provides the design of the monitoring system, including the state-space modelling of the physical systems, the residual generation, the adaptive threshold and the decision logic. Simulation results are provided in Section 4, followed by concluding remarks and directions for future research.

2. Offshore heavy lift construction modelling

In this section, the mode detection problem is defined. The physical model of the interconnected system (i.e., crane vessel with the load) is given at the end.

During an offshore removal construction work, there are commonly two steps. During the first step, the vessel lifts the load from the platform (Mode 2 in Fig. 2), which takes about 10–30 min. During the second step (i.e., Mode 1 in Fig. 2), the load is lifted from the platform and suspended in the air. In the first step, the load is assumed to be fixed on the platform with limitation of movements. While during the second step, the load is assumed to be able to move in 3 DoFs (i.e., in the directions of north, east, and down). The dynamics of the vessel-load system are different within first and second step.

Following notations are used throughout the paper: $|\cdot|$ and $\|\cdot\|$ represent the element-wise absolute value and the Euclidean norm respectively; $\mathbf{I}$ denotes identity matrix with appropriate dimension; $\mathbf{0}_j$ and $\mathbf{I}_j$ denote the zero and identity matrix of dimension j respectively; $diag\{\cdot,\cdots,\cdot\}$ denotes a diagonal matrix with diagonal elements $\{\cdot,\cdots,\cdot\}$; bold letters represent vectors and matrices.

Under the assumption that the vessel's offset and rotation angles are kept small with low velocity and acceleration by the DP system, the motion of a crane vessel assuming 6 DoFs can be expressed as (Fossen, 2011):

$$\mathbf{M}\dot{\boldsymbol{\nu}}(t) + \mathbf{D}\boldsymbol{\nu}(t) + \mathbf{C}(\boldsymbol{\nu}(t))\boldsymbol{\nu}(t) + \mathbf{G}(\boldsymbol{\eta}(t)) + \mathbf{g} = \tau_{th}(t) + \tau_e(t) + \tau_1(t), \tag{1}$$

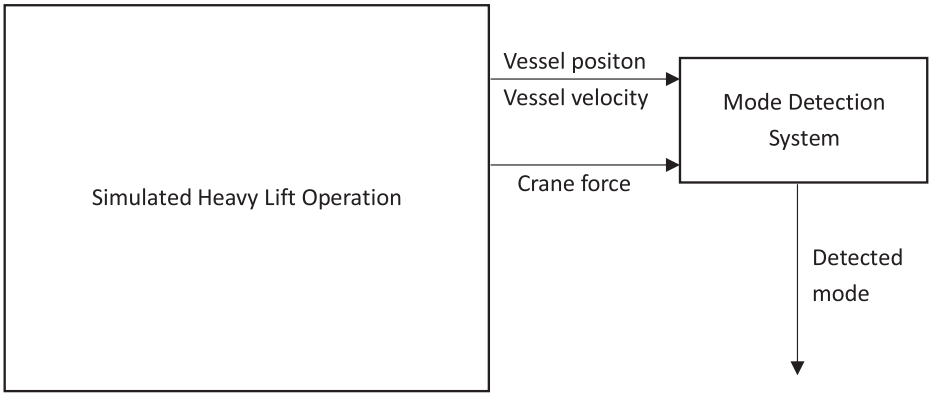

Fig. 1. Mode Detection System for Offshore Heavy Lift Operation.

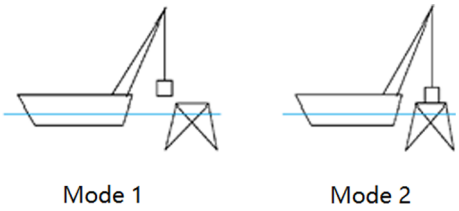

Fig. 2. Two Modes for Offshore Assignment.

$$\dot{\eta}(t) = \mathbf{R}(\phi, \theta, \psi)\nu(t), \tag{2}$$

where $\nu = [u, v, w, p, q, r]^T$ is the vessel's velocity in the body-fixed coordinate system; $\eta = [x, y, z, \phi, \theta, \psi]^T$ is the vessel position in North-East-Down coordinate system (NED); the signal $\tau_{th} \in \mathbb{R}^6$ is the force and moment given by the propulsion system; $\tau_e \in \mathbb{R}^6$ denotes the environmental forces and moments which are induced due to current, wind and wave; $\tau_l = [\mathbf{F}_l, \mathbf{T}_l]^T$ is the force and moment resulting from the crane load, with $\mathbf{F}_l \in \mathbb{R}^3$, $\mathbf{T}_l = \mathbf{r}_{ct} \times \mathbf{F}_l$, where $\mathbf{r}_{ct} \in \mathbb{R}^3$ is the vector from vessel's Center of Rotation to the crane tip; and the term $\mathbf{R} \in \mathbb{R}^{6\times6}$ is the transfer matrix from vessel's body-fixed to NED coordinate system; $\mathbf{M} \in \mathbb{R}^{6\times6}$ is the mass matrix of the crane vessel; $\mathbf{D} \in \mathbb{R}^{6\times6}$ is the damping matrix; $\mathbf{C} \in \mathbb{R}^{6\times6}$ is the Coriolis matrix; $\mathbf{g} = [0, 0, -M_v g, 0, 0, 0]^T$ is the mass gravity of the vessel, in which M_v is the vessel mass and g is the gravity acceleration; $\mathbf{G}(\eta)$ refers to the hydrostatic force on the vessel. The details of τ_e can be found in Fossen (2011). The crane wire is modeled as a spring-damper system, and the winch is modeled as a hydraulic system as in Ye et al. (2019).

During the removal procedure, the dynamics of the vessel-load system are different in the second construction mode compared to the first mode. During the second mode, the vessel can be considered as moored to the platform with the force controlled by a hydraulic winch system. During the first construction mode, the vessel and the load can be considered as two objects connected by the crane wires, which could be modeled as a spring-damper system. Modelling of these two modes are given below.

2.1. Construction mode 1

When the load is suspended, the vessel and the load could be seen as connected by the hoist wire. As the load's rotation has less impact on vessel's position stability compared to the impact from its position control, the load dynamics can be simplified to 3 DoFs:

$$\mathbf{M}_l\ddot{\eta}_l(t) + \mathbf{D}_l\dot{\eta}_l(t) + \mathbf{g}_l = \mathbf{F}_{\text{env}}(t) - \mathbf{R}_3(\phi, \theta, \psi)\mathbf{F}_l(t), \tag{3}$$

where η_l is the position of the load in NED; $\mathbf{M}_l \in \mathbb{R}^{3\times3}$ is the mass matrix of the load; $\mathbf{D}_l \in \mathbb{R}^{3\times3}$ is the damping matrix of the load; $\mathbf{g}_l = [0, 0, -M_l g]^T$ is the mass gravity of the load, in which M_l is the mass of the load; and $\mathbf{R}_3 \in \mathbb{R}^{3\times3}$ is the rotation matrix from Body-fixed coordinate system (BODY) to NED in 3 DoFs.

The force induced by the load can be expressed as:

$$\mathbf{F}_l(t) = \frac{F_{\text{hoist}}(t)}{||\delta_l(t)||}\delta_l(t), \tag{4}$$

where

$$F_{\text{hoist}}(t) = \begin{cases} (K_{\text{wires}}\ \tilde{\delta}(t) + D_{\text{wires}}\dot{\tilde{\delta}}(t)), & \text{if } \tilde{\delta}(t) > 0; \\ 0, & \text{if } \tilde{\delta}(t) \leqslant 0. \end{cases} \tag{5}$$

In Eq. (5),

$$\tilde{\delta}(t) = ||\delta_l(t)|| - ||\delta_l(0)|| \tag{6}$$

is the elastic elongation of the crane wires;

$$\delta_l(t) = \mathbf{p}_l(t) - \mathbf{p}_{\text{ct}}, \tag{7}$$

with $\mathbf{p}_{\text{ct}} = [x_{ct}, y_{ct}, z_{ct}]^T$ being the constant vector that denotes the position of crane-tip and $\mathbf{p}_l = [x_l, y_l, z_l]^T$ is the load position in vessel's body-fixed coordinate system, which satisfies

$$\mathbf{p}_l = \mathbf{R}_3^T(\phi, \theta, \psi)(\eta_l - \eta_3), \tag{8}$$

where $\eta_3 = [x, y, z]^T$ is the vector of the first three elements of η.

2.2. Construction mode 2

During mode 2, the position of the load in NED is assumed to be constant, i.e., $\dot{\eta}_l = \mathbf{0}$. The lifting and dropping of the crane load is controlled by a hydraulic winch, i.e., F_{hoist} in (4) is controlled by a hydraulic winch (Zhang, 2008).

Remark 1. Current DP systems for crane vessels are widely designed and tuned assuming no load. Particularly, they are designed based on (1) and (2) assuming that τ_l is zero. Thus the position stability of the crane vessel may be jeopardized when activating the hydraulic winch to lift up the load. To address the position stability issue by switching to another controller for DP, we need to determine the time of the switching between the two modes as soon as possible. Currently, the switching is detected by a human operator or a robot, if the load is under water by visually observing whether the structure is lifted up or not. The fact that in this approach there should be visual contact and communication between human operators may impose time delays that depend on the experience of human operators (or robots in case of loads under water) and their performance under various environmental conditions (Ye, 2016).

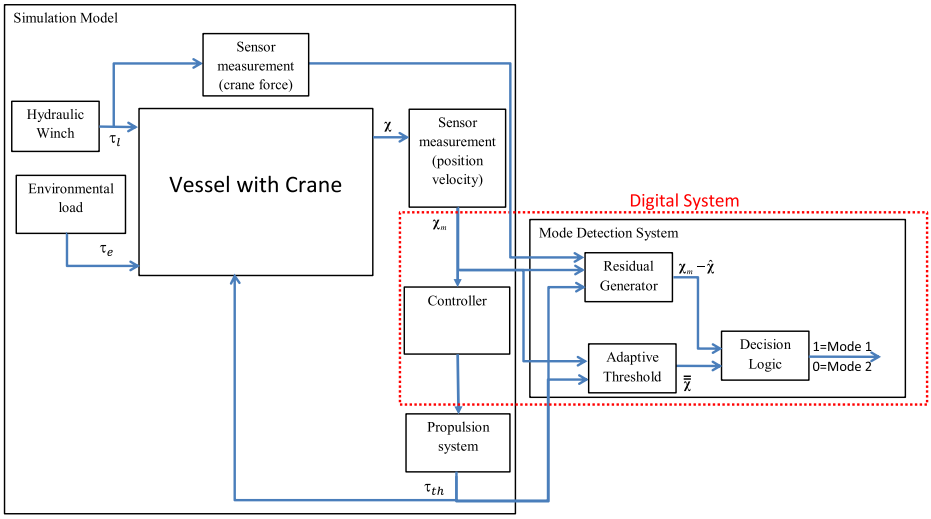

Fig. 3. Overall Detection System.

3. Construction mode detection

This section provides the design of a decision-support monitoring system responsible for detecting the changes between both modes, assuming that there are available sensors to provide measurements of the position and velocity of the crane vessel, and the measurements of the tension force of the lifting wires. The detection system can support the decision making process of the human operators. An overview of the monitoring system is shown in Fig. 3. The inputs to this system are the sensor measurements and the controlled thrust force of the crane vessel. The output of this system is the decision about the construction mode, i.e., binary decision with 0 and 1 corresponding to "mode 2" (load-on-platform) and "mode 1" (load-suspended) respectively.

For designing this system, we follow a model-based approach, where we express the equations of motion of the crane vessel and the heavy load in a state-space content. The dependence of signals on time is dropped for simplicity, and only when new variables are introduced, it will be highlighted. The state space representation is derived by considering the DP of the crane vessel and the lifting of the heavy load by the wires as two interconnected operations; i.e., based on (1) and (2), we obtain the following state-space system:

$$\Sigma^{(1)}: \dot{\chi}^{(1)} = \mathbf{A}^{(1)}\chi^{(1)} + \gamma^{(1)}(\chi^{(1)}, \mathbf{u}^{(1)}) + h^{(1)}(\chi^{(1)}, \mathbf{u}^{(1)}, \zeta^{(1)}, u_{\zeta}^{(1)}) + \omega_1^{(1)}, \tag{9}$$

$$\Sigma^{(2)}: \dot{\chi}^{(2)} = \mathbf{A}^{(2)}\chi^{(2)} + \gamma^{(2)}(\chi^{(2)}, \mathbf{u}^{(2)}) + h^{(2)}(\chi^{(2)}, \mathbf{u}^{(2)}, \zeta^{(2)}, \mathbf{u}_{\zeta}^{(2)}) + \omega_1^{(2)}, \tag{10}$$

where $\Sigma^{(1)}$ denotes the first system (i.e., the vessel dynamics), and $\Sigma^{(2)}$ denotes the second system (i.e., the load dynamics). with

$$\chi^{(1)} = \begin{bmatrix}\eta \\ \nu\end{bmatrix}, \mathbf{u}^{(1)} = \tau_{th}, \zeta^{(1)} = [\mathbf{I}_3 \quad \mathbf{0}_3 \quad \mathbf{0}]\chi^{(2)}, \mathbf{u}_{\zeta}^{(1)} = F_{\text{hoist}}, \tag{11}$$

$$\chi^{(2)} = \begin{bmatrix}\eta_l \\ \nu_l \\ \tilde{\delta}\end{bmatrix}, \mathbf{u}^{(2)} = F_{\text{hoist}}, \zeta^{(2)} = [\mathbf{I}_3 \quad \mathbf{0}_3 \quad 0_6]\chi^{(1)}, \mathbf{u}_{\zeta}^{(2)} = 0. \tag{12}$$

The first two terms of (9) and (10) describe the local known dynamics while the third term h represents the interconnection dynamics, and ω_1 is the disturbance signal which induced by the environmental disturbances. For $\Sigma^{(1)}$,

$$\mathbf{A}^{(1)} = \begin{bmatrix}\mathbf{0} & \mathbf{0} \\ -\mathbf{M}^{-1}\mathbf{G} & -\mathbf{M}^{-1}\mathbf{D}\end{bmatrix}, \tag{13}$$

$$\gamma^{(1)}(\chi^{(1)}, \mathbf{u}^{(1)}) = \begin{bmatrix}\mathbf{R}(\eta)\nu \\ \mathbf{M}^{-1}(-\mathbf{C}(\nu)\nu + \mathbf{u}^{(1)} - \mathbf{g})\end{bmatrix}, \tag{14}$$

$$\omega_1^{(1)} = \begin{bmatrix}\mathbf{0} \\ \mathbf{M}^{-1}\tau_e\end{bmatrix}. \tag{15}$$

The interconnection term in $\Sigma^{(1)}$ can be expressed as:

$$h^{(1)}(\chi^{(1)}, \mathbf{u}^{(1)}, \zeta^{(1)}, u_{\zeta}^{(1)}) \tag{16}$$

$$= \begin{bmatrix}\mathbf{0} \\ \mathbf{M}^{-1}\tau_l\end{bmatrix} = \begin{bmatrix}\mathbf{0} \\ \mathbf{M}^{-1}\begin{bmatrix}\mathbf{F}_l \\ \mathbf{T}_l\end{bmatrix}\end{bmatrix} \tag{17}$$

$$= \begin{bmatrix}\mathbf{0} \\ \mathbf{M}^{-1}\begin{bmatrix}\frac{F_{\text{hoist}}}{\| \mathbf{R}_3^T(\eta)(\eta_l - \eta_3) - \mathbf{p}_{\text{ct}} \|}(\mathbf{R}_3^T(\eta)(\eta_l - \eta_3) - \mathbf{p}_{\text{ct}}) \\ \frac{F_{\text{hoist}}}{\| \mathbf{R}_3^T(\eta)(\eta_l - \eta_3) - \mathbf{p}_{\text{ct}} \|}\mathbf{r}_{ct} \times (\mathbf{R}_3^T(\eta)(\eta_l - \eta_3) - \mathbf{p}_{\text{ct}})\end{bmatrix}\end{bmatrix}, \tag{18}$$

where F_{hoist} is controlled by the winch during mode 2, or is an uncontrolled force created by the connection through the wires in mode 1 described by (5).

For $\Sigma^{(2)}$, during mode 2, the load position is fixed, thus $\dot{\chi}^{(2)} = \mathbf{0}$, and $\eta_l = \eta_l^{\circ}$, where η_l° is constant.

The behavior of $\Sigma^{(2)}$ in mode 1 can be expressed by (10) with

$$\mathbf{A}^{(2)} = \begin{bmatrix}\mathbf{0} & \mathbf{I} & \mathbf{0} \\ \mathbf{0} & -\mathbf{M}_l^{(-1)}\mathbf{D}_l & \mathbf{0} \\ \mathbf{0} & \mathbf{0} & -\frac{K_{\text{wires}}}{D_{\text{wires}}}\end{bmatrix}, \tag{19}$$

$$\gamma^{(2)}(\chi^{(2)}, \mathbf{u}^{(2)}) = \begin{bmatrix}\mathbf{0} \\ -\mathbf{M}^{(-1)}\mathbf{g}_l \\ \frac{u^{(2)}}{D_{\text{wires}}}\end{bmatrix}. \tag{20}$$

$$\omega_1^{(2)} = \begin{bmatrix}\mathbf{0} \\ \mathbf{M}_l^{(-1)}\mathbf{F}_{\text{env}} \\ 0\end{bmatrix}. \tag{21}$$

The interconnection term in $\Sigma^{(2)}$ can be expressed as:

$$h^{(2)} = \begin{bmatrix}\mathbf{0} \\ \frac{F_{\text{hoist}}}{\| \mathbf{R}_3(\eta)\mathbf{p}_{\text{ct}} - \eta_l \|}\mathbf{M}^{(-1)}(\mathbf{R}_3(\eta)\mathbf{p}_{\text{ct}} - \eta_l) \\ 0\end{bmatrix}. \tag{22}$$

In order to detect the switching of the construction mode, we select to monitor a feature that is expected to change during the switching. This feature is a residual vector that corresponds to the difference between the observed behavior (measured internal state) of system $\Sigma^{(1)}$ denoted by $\chi_m \in \mathbb{R}^{12}$ and its expected behavior denoted by $\hat{\chi}(t) \in \mathbb{R}^{12}$ that is the estimation of its state by a nonlinear observer (a software-based system that provides an estimation of the internal state of a real system using its input and output signals). A model-based nonlinear observer is designed for the vessel's position and velocity estimation during mode 2, i.e., $\eta_1 = \eta^\circ$, based on (9), (11), and (13)-(18). The residual $\chi_m - \hat{\chi}$ is then compared to the adaptive threshold denoted by $\bar{\tilde{\chi}}(t) \in \mathbb{R}^{12}$. If the magnitude of one or more residual is larger than the adaptive boundary, then it is inferred that the construction mode is 1, meaning that the load is lifted up. The designed nonlinear observer, adaptive threshold, and decision logic are described separately in this section.

3.1. Residual generation

For simplicity of the notation, we drop the superscript $^{(1)}$ in the following equations. The nonlinear observer is designed as:

$$\dot{\hat{\chi}} = \mathbf{A}\hat{\chi} + \gamma(\chi_m, \mathbf{u}) + h(\chi_m, \mathbf{u}, \zeta, \mathbf{u}_\zeta) + \mathbf{K}(\chi_m - \hat{\chi}) \tag{23}$$

$$\zeta = \eta_1 = \eta_1^\circ \tag{24}$$

where $\hat{\chi}(t) \in \mathbb{R}^{12}$ is the estimated states, $\chi_m(t) = [\eta_m, \nu_m]^T \in \mathbb{R}^{12}$ is the measurement of the vessel position and vessel velocity, the measurement

$$\chi_m = \chi + \omega_2, \tag{25}$$

where $\omega_2(t) = [\omega_\eta, \omega_\nu]^T \in \mathbb{R}^{12}$ is the measurement noise, and $\mathbf{K} \in \mathbb{R}^{12\times 12}$ is the observer gain.

By using (9), (13)-(18) and (23), the state estimation error dynamics can be expressed as

$$\begin{aligned}\dot{\tilde{\chi}} &= (\mathbf{A} - \mathbf{K})\tilde{\chi} + (\gamma(\chi, \mathbf{u}) - \gamma(\chi_m, \mathbf{u})) \\ &+ (h(\chi, \mathbf{u}, \zeta, \mathbf{u}_\zeta) - h(\chi_m, \mathbf{u}, \zeta, \mathbf{u}_\zeta)) + \omega_1 - \mathbf{K}\omega_2,\end{aligned} \tag{26}$$

where

$$\tilde{\chi}(t) = \chi(t) - \hat{\chi}(t). \tag{27}$$

For the stability of the observer, the gain $\mathbf{K}$ should be chosen such that matrix $\mathbf{A} - \mathbf{K}$ is Hurwitz Matrix as we analyze next.

By using (25), (27), the residual vector $\chi_m - \hat{\chi}$ can be described with respect to the state estimation error as

$$\chi_m(t) - \hat{\chi}(t) = \tilde{\chi}(t) + \omega_2(t) \tag{28}$$

Remark 2. Considering the dynamic positioning system and the lifting of the load as two interconnected operations enabled us to design a state-space observer given in (23) for the crane-vessel dynamics, i.e., for $\Sigma^{(1)}$ including only the dynamics of the system $\Sigma^{(2)}$ that affect $\Sigma^{(1)}$ due to interconnection modeled by h. In this way, we have an observer of order 12 instead of an observer of order 19, which could be designed if we follow a centralized approach to estimate the state $[\chi^{(1)}; \chi^{(2)}]$ of the crane-vessel-load system. This leads to smaller number of residuals and corresponding adaptive thresholds that should be checked online according to the decision logic presented in Section 3.3.

3.2. Adaptive threshold

Due to the presence of disturbances and measurement noise (i.e., ω_1 and ω_2), the observed behavior always deviates from the expected one, which means that the residual will never be zero. To detect the change of the construction mode through the residual vector $\chi_m(t) - \hat{\chi}(t)$, we compare at every time instant the residual vector to an adaptive threshold vector $\bar{\tilde{\chi}}(t)$. This adaptive threshold vector is obtained assuming:

- the crane vessel and the heavy load are operating in mode 2;
- the disturbances and the measurement noise are unknown but bounded, i.e., $|\omega_1(t)| \leqslant \bar{\omega}_1$ and $|\omega_2(t)| \leqslant \bar{\omega}_2$ for all $t > 0$ with $\bar{\omega}_1$ and $\bar{\omega}_2$ being positive constants;
- the position of the crane load during the mode 2 and the tension in the crane wires are exactly known.

The adaptive threshold is computed such that:

$$|\chi_m(t) - \hat{\chi}(t)| \leqslant \bar{\tilde{\chi}}(t), \tag{29}$$

where $\bar{\tilde{\chi}}(t) \in \mathbb{R}^{12}$ is the adaptive threshold of the detection system.

Using (26) and applying the triangular inequality results in:

$$|\chi_m(t) - \hat{\chi}(t)| \leqslant |\tilde{\chi}(t)| + \bar{\omega}_2(t),$$

where
$\bar{\omega}_2(t) = [\bar{\omega}_\eta(t), \bar{\omega}_\nu(t)] = [\bar{\omega}_x, \bar{\omega}_y, \bar{\omega}_z, \bar{\omega}_\phi, \bar{\omega}_\theta, \bar{\omega}_\psi, \bar{\omega}_u, \bar{\omega}_v, \bar{\omega}_w, \bar{\omega}_p, \bar{\omega}_q, \bar{\omega}_r]$ is the measurement noise bound. Define the adaptive threshold as

$$\bar{\chi}(t) + \bar{\omega}_2(t) \triangleq \bar{\tilde{\chi}}(t) \tag{30}$$

where $\bar{\chi}(t) \in \mathbb{R}^{12}$ is the adaptive bound on the state estimation error, i.e.,

$$|\tilde{\chi}| \leqslant \bar{\chi}, \tag{31}$$

The bound $\bar{\chi}$ can be calculated by solving the differential equation and applying the triangular inequality as described in Appendix A. The adaptive bound $\bar{\chi}$

$$\bar{\chi}(t) = e^{\lambda t}\bar{\chi}(0) + [-\lambda^{-1}(\mathbf{I} - e^{\lambda t})(\bar{\omega}_1 + |\mathbf{K}|\bar{\omega}_2)] + \mathbf{H}(s)(\bar{\gamma}(t) + \bar{h}(t)), \tag{32}$$

where $\bar{\chi}(0)$ is the upper bound for the initial estimation error, $\bar{\omega}_1 \in \mathbb{R}^{12}$ is bound for the environmental load, $\lambda = diag\{\lambda_1, \lambda_2, \cdots, \lambda_{12}\}$ is the diagonal matrix with the real negative eigen values of $\mathbf{A} - \mathbf{K}$, $\mathbf{H}(s)$ is a stable first-order filter defined by elements in λ (see Isermann, 2006), i.e.,

$$\mathbf{H}(s) = diag\{H_1(s), \cdots, H_{12}(s)\}, \tag{33}$$

where

$$H_i(s) = \frac{1}{s - \lambda_i}, \lambda_i < 0; \tag{34}$$

and $\bar{\gamma}(t) \in \mathbb{R}^{12}$ is the adaptive bound on $|\gamma(\chi, \mathbf{u}) - \gamma(\chi_m, \mathbf{u})|$, $\bar{h}(t) \in \mathbb{R}^{12}$ is the adaptive bound on $|h(\chi, \mathbf{u}, \zeta, \mathbf{u}_\zeta) - h(\chi_m, \mathbf{u}, \zeta, \mathbf{u}_\zeta)|$ defined as:

$$\bar{\gamma}(\bar{\omega}_2, \chi_m) = \begin{bmatrix} [||[\bar{\omega}_{\nu 1}, \bar{\omega}_{\nu 2}, \bar{\omega}_{\nu 3}]||[1, 1, 1], ||[\bar{\omega}_{\nu 4}, \bar{\omega}_{\nu 5}, \bar{\omega}_{\nu 6}]||[1, 1, 1]]^T + \\ |\bar{\mathbf{R}}(\bar{\omega}_\eta)\nu_m(t)| \\ \mathbf{M}^{-1}\bar{\mathbf{C}} \end{bmatrix}, \tag{35}$$

$$\bar{h}(\bar{\omega}_2, \chi_m) = \begin{bmatrix} \mathbf{0} \\ \mathbf{M}^{-1}\bar{\tau}_1 \end{bmatrix}, \tag{36}$$

where

$$\bar{\mathbf{C}} = \bar{\mathbf{C}}_1(\bar{\omega}_\nu) + |\bar{\mathbf{C}}_2(\bar{\omega}_\nu)\nu_m(t)|, \tag{37}$$

$$\bar{\tau}_1 = \begin{bmatrix} F_{\text{hoist}}\bar{\beta} \\ \mathbf{r}_{ct} \times F_{\text{hoist}}\bar{\beta} \end{bmatrix}. \tag{38}$$

In (35),

$$\bar{\mathbf{R}}(\bar{\omega}_\eta) = \begin{bmatrix} \bar{\omega}_\theta + \bar{\omega}_\phi & \bar{\omega}_\theta + 2\bar{\omega}_\phi + 2\bar{\omega}_\psi & \bar{\omega}_\theta + 2\bar{\omega}_\phi + 2\bar{\omega}_\psi & 0 & 0 & 0 \\ \bar{\omega}_\theta + \bar{\omega}_\psi & \bar{\omega}_\theta + 2\bar{\omega}_\phi + 2\bar{\omega}_\psi & \bar{\omega}_\theta + 2\bar{\omega}_\phi + 2\bar{\omega}_\psi & 0 & 0 & 0 \\ \bar{\omega}_\theta & \bar{\omega}_\theta + 2\bar{\omega}_\phi + 2\bar{\omega}_\psi & \bar{\omega}_\theta + 2\bar{\omega}_\phi + 2\bar{\omega}_\psi & 0 & 0 & 0 \\ 0 & 0 & 0 & 0 & \frac{\bar{\omega}_\phi + 2\bar{\omega}_\theta}{1 - 2\bar{\omega}_\theta} & \frac{\bar{\omega}_\phi + 2\bar{\omega}_\theta}{1 - 2\bar{\omega}_\theta} \\ 0 & 0 & 0 & 0 & \bar{\omega}_\phi & \bar{\omega}_\phi \\ 0 & 0 & 0 & 0 & \frac{\bar{\omega}_\phi + \bar{\omega}_\theta}{1 - 2\bar{\omega}_\theta} & \frac{\bar{\omega}_\phi + \bar{\omega}_\theta}{1 - 2\bar{\omega}_\theta} \end{bmatrix}. \tag{39}$$

In (37),

$$\bar{\mathbf{C}}_1(\bar{\omega}_\nu) = \begin{bmatrix} m(\bar{\omega}_w\bar{\omega}_q + \bar{\omega}_v\bar{\omega}_r + z_g\bar{\omega}_q\bar{\omega}_r) \\ m(\bar{\omega}_w\bar{\omega}_p + \bar{\omega}_u\bar{\omega}_r + z_g\bar{\omega}_p\bar{\omega}_r) \\ m(\bar{\omega}_v\bar{\omega}_p + \bar{\omega}_u\bar{\omega}_q + 2z_g\bar{\omega}_p\bar{\omega}_q) \\ (I_z + I_y)\bar{\omega}_r\bar{\omega}_q + mz_g(\bar{\omega}_u\bar{\omega}_r + \bar{\omega}_w\bar{\omega}_p) \\ (I_z + I_x)\bar{\omega}_p\bar{\omega}_r + mz_g\bar{\omega}_r\bar{\omega}_v \\ (I_x + I_y)\bar{\omega}_p\bar{\omega}_q \end{bmatrix}, \tag{40}$$

$$\bar{\mathbf{C}}_2(\bar{\omega}_\nu) = \begin{bmatrix} 0 & m\bar{\omega}_r & m\bar{\omega}_q & 0 \\ m\bar{\omega}_r & 0 & m\bar{\omega}_p & m(\bar{\omega}_w + z_g\bar{\omega}_r) \\ m\bar{\omega}_q & m\bar{\omega}_p & 0 & m(\bar{\omega}_v + z_g\bar{\omega}_q) \\ mz_g\bar{\omega}_r & 0 & mz_g\bar{\omega}_p & mz_g\bar{\omega}_w \\ 0 & mz_g\bar{\omega}_r & 0 & (I_x + I_z)\bar{\omega}_r \\ 0 & 0 & 0 & (I_x + I_y)\bar{\omega}_q \end{bmatrix} \tag{41}$$

$$\begin{bmatrix} m(\bar{\omega}_w + z_g\bar{\omega}_r) & m(\bar{\omega}_v + z_g\bar{\omega}_q) \\ 0 & m(\bar{\omega}_u + z_g\bar{\omega}_p) \\ m(\bar{\omega}_u + z_g\bar{\omega}_p) & 0 \\ (I_y + I_z)\bar{\omega}_r & (I_y + I_z)\bar{\omega}_q + mz_g\bar{\omega}_u \\ 0 & (I_x + I_z)\bar{\omega}_p + mz_g\bar{\omega}_v \\ (I_x + I_y)\bar{\omega}_p & 0 \end{bmatrix}. \tag{42}$$

In (38),

$$\bar{\beta} = \frac{|\mathbf{R}_3^T(\eta_m)(\eta_1 - \eta_{3m}) - \mathbf{p}_{ct}| + |\mathbf{R}_3^T\eta_1| + \|\bar{\omega}_{3\eta}\|[1,1,1]^T + |\mathbf{R}_3^T\eta_m|}{\|\|(\eta_1 - \eta_{3m}) - \mathbf{R}_3(\eta_m)\mathbf{p}_{ct}\| - \|\bar{\omega}_{3\eta}\| - \|\bar{\mathbf{R}}_3\mathbf{p}_{ct}\|\|} - \frac{\mathbf{R}_3^T(\eta_m)(\eta_1 - \eta_{3m}) - \mathbf{p}_{ct}}{\|\mathbf{R}_3^T(\eta_m)(\eta_1 - \eta_{3m}) - \mathbf{p}_{ct}\|}. \tag{43}$$

where $\bar{\omega}_{3\eta} = [\bar{\omega}_x, \bar{\omega}_y\bar{\omega}_z]^T$, and

$$\bar{\mathbf{R}}_3(\bar{\omega}_\eta) = \begin{bmatrix} \bar{\omega}_\theta + \bar{\omega}_\phi & \bar{\omega}_\theta + 2\bar{\omega}_\phi + 2\bar{\omega}_\psi & \bar{\omega}_\theta + 2\bar{\omega}_\phi + 2\bar{\omega}_\psi \\ \bar{\omega}_\theta + \bar{\omega}_\psi & \bar{\omega}_\theta + 2\bar{\omega}_\phi + 2\bar{\omega}_\psi & \bar{\omega}_\theta + 2\bar{\omega}_\phi + 2\bar{\omega}_\psi \\ \bar{\omega}_\theta & \bar{\omega}_\theta + 2\bar{\omega}_\phi + 2\bar{\omega}_\psi & \bar{\omega}_\theta + 2\bar{\omega}_\phi + 2\bar{\omega}_\psi \end{bmatrix}. \tag{44}$$

Details of (30), (33)-(44) can be found in Appendix A, Appendix B, and Appendix C.

Remark 3. The implemented adaptive threshold is described by (30), (32)-(44). Note that in the upper half of (35) the first term is constant and $\bar{\mathbf{R}}$ in the second term is constant, both are functions of the noise bound. Similar for (37), the first term and $\bar{\mathbf{C}}_2$ in the second term are also constant. If the noise is zero, then the adaptive threshold becomes:

$$\bar{\tilde{\chi}}(t) = e^{\lambda t}\bar{\chi}(0) + [-\lambda^{-1}(\mathbf{I} - e^{\lambda t})\bar{\omega}_1].$$

3.3. Detection decision logic

The transition from mode 2 to mode 1 is detected at the first time instant that,

$$|\hat{\chi}(t) - \chi_m(t)| > \bar{\tilde{\chi}}(t) \tag{45}$$

that is if one or more elements of the vector $|\hat{\chi}(t) - \chi_m(t)|$, and we infer that the construction mode has changed to free-hanging. By the design of the residual and the adaptive threshold, if

$$|\hat{\chi}(t) - \chi_m(t)| \leqslant \bar{\tilde{\chi}}(t) \tag{46}$$

is satisfied for all elements in $|\hat{\chi}(t) - \chi_m(t)|$, the interconnected system is inferred to operate in mode 2. The detected switching time is defined as:

$$t_D = min\{t_{Dj}: j \in 1, 2, 3, ..., 12\}, \tag{47}$$

$$t_{Dj} = min\{t: |\hat{\chi}(t) - \chi_m(t)| > \bar{\tilde{\chi}}(t)\}.$$

The detection time delay is defined as:

$$\tilde{t} = t_D - t_s, \tag{48}$$

where t_s is the actual mode switching time. Note that the validity of (47) and (48) is checked at every time instant.

Remark 4. The proposed mode detection scheme does not depend on the characteristics of the load or the wires. The mode detection scheme shown in Fig. 3 can be embedded as a software-based module implemented in the digital computer used for the DP of the vessel, and there is no need to change its parameters every time that the crane vessel should lift a new load. If we have followed a centralized approach treating $\Sigma^{(1)}$ and $\Sigma^{(2)}$ as one system and design an observer for the augmented system, then it would be necessary to change the design parameters of the detection system with respect to the characteristics of the load.

Remark 5. The use of adaptive threshold instead of a fixed threshold reduces the conservativeness in the decision-making process. A fixed threshold could be simpler in its real implementation but its determination would require a large amount of historical data during mode 2 before using the threshold in the detection scheme.

4. Simulation results

In this section, we present simulation results that are performed with a payload of 2400 tonnes under sea state 2. Sea state is an oceanographic way to describe the condition of the water surface on a large scale with respect to wind and waves at certain location and time. Sea state 2 describes a slight sea condition, with wavelets on the ocean water surface. The simulations in this section are made with a significant wave height of 0.5 m, current speed of 0.6 m/s, and wind velocity of 2.5 m/s. Details of the controller and the simulated vessel (e.g., mass matrix, damping matrix, data and modelling details for hydraulic winch and the crane wires etc.) can be found in Ye et al. (2019),Ye et al. (2020). The environmental disturbances come from 30° east of south. As described in the beginning of Section 3.2, the simulated bounds on the system disturbance and measurement noise are:

$$\bar{\omega}_1 = 0.01[0 \;\; 0 \;\; 0 \;\; 0 \;\; 0 \;\; 0 \;\; 2 \;\; 6 \;\; 0.1 \;\; 0.1 \;\; 0.01 \;\; 0.1]^T, \tag{49}$$

$$\bar{\omega}_2 = 0.1\left[1 \;\; 1 \;\; 1 \;\; 1 \;\; 1 \;\; 1 \;\; \frac{\pi}{180} \;\; \frac{\pi}{180} \;\; \frac{\pi}{180} \;\; \frac{\pi}{180} \;\; \frac{\pi}{180} \;\; \frac{\pi}{180}\right]^T. \tag{50}$$

The observer gain $\mathbf{K}$ in (23) has been selected such that the eigenvalues of the matrix are:

$$\lambda = -0.1 \times diag\{1 \;\; 1 \;\; 1 \;\; 1 \;\; 1 \;\; 1 \;\; 0.5 \;\; 4 \;\; 10 \;\; 10 \;\; 5 \;\; 3\}. \tag{51}$$

The simulation consists of three steps with switching time at $t_s = 600$ s, and a total simulation time of 800 s:

- During the first 50 s, there's no crane load on the vessel;
- Mode 2: From 50 s up to 600 s, the vessel is lifting the load, and

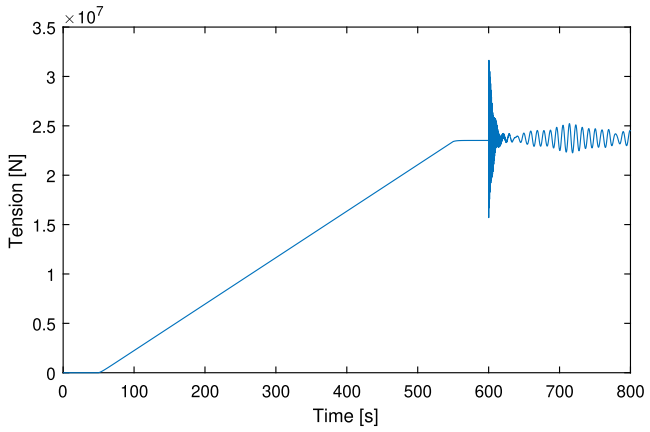

Fig. 4. Tension in the Crane Wires during the Simulation.

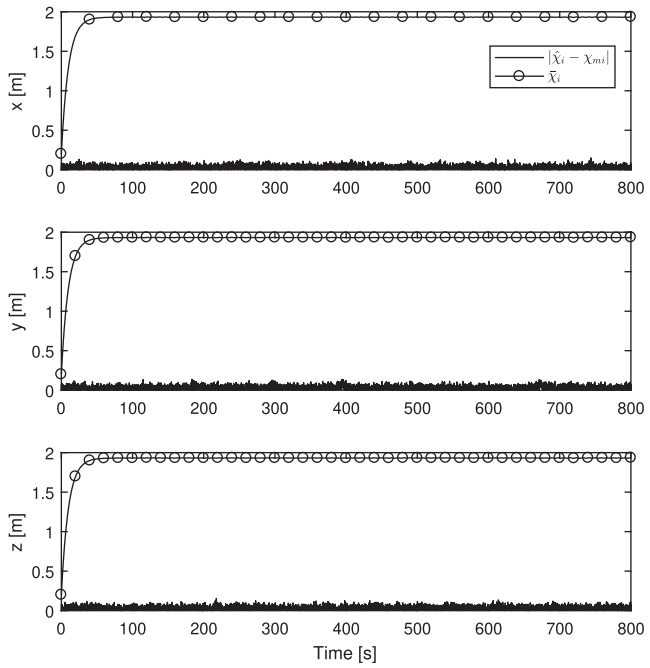

Fig. 5. Residual ($|\hat{\chi}_i - \chi_{mi}|$) and adaptive threshold ($\bar{\chi}_i$) for $i = 1$, 2, and 3.

could be seen as moored to the platform via crane wires with increasing crane load;

- Mode 1: From 600 s to 800 s, the load is fully lifted and is free-hanging.

The tension in the crane wires during the simulation is shown in Fig. 4. From 50 s to 600 s (i.e., during Mode 2), F_{hoist} is controlled by a hydraulic winch with a linearly increasing input. The position of the vessel is controlled by a DP system with a maximum position error less than 0.2 m, limiting significantly the oscillations in the tension force.

The mode detection scheme is designed as shown in Section 3, where the nonlinear observer in (23)-(24) is structured using (51) and $\eta_1 = [-115,\ 0,\ -9.19]^T$. The adaptive thresholds are designed using (49) and (50) as the bounds on the disturbances and measurement noise respectively. The bound on the initial condition is set to

$$\bar{\chi}(0) = 0.1[1\ \ 1\ \ 1\ \ 1\ \ 1\ \ 1\ \ 1\ \ 1\ \ 1\ \ 1\ \ 1\ \ 1]^T \tag{52}$$

Figs. 5–8 show the magnitude of the residual $|\chi_{mi}(t) - \hat{\chi}_i(t)|$ and the adaptive threshold $\bar{\chi}_i(t)$ during the simulation. Fig. 9 shows the actual

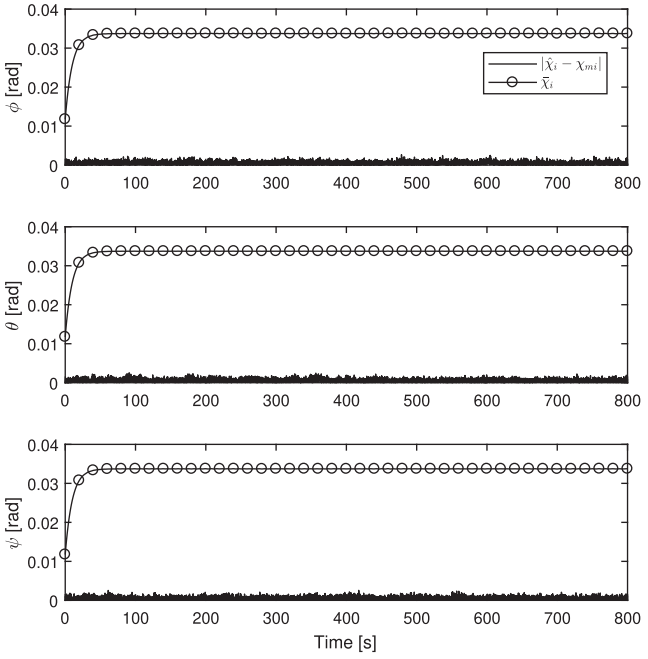

Fig. 6. Residual ($|\hat{\chi}_i - \chi_{mi}|$) and adaptive threshold ($\bar{\chi}_i$) for $i = 4$, 5, and 6.

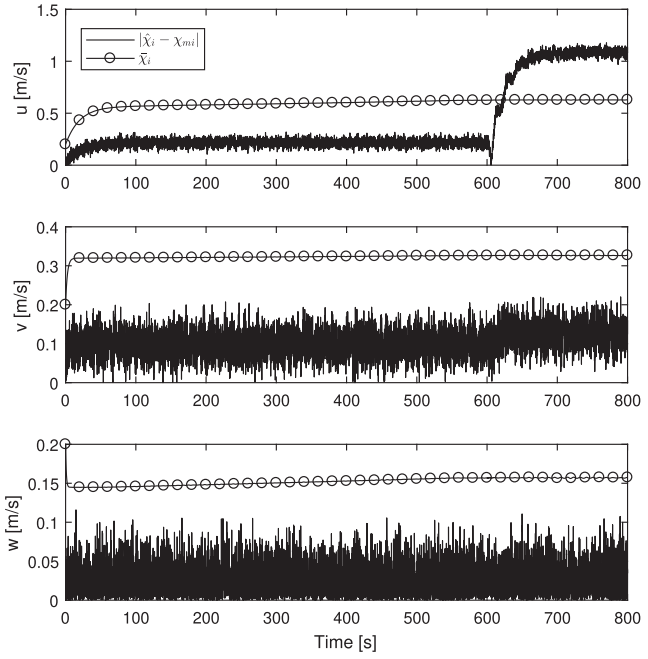

Fig. 7. Residual ($|\hat{\chi}_i - \chi_{mi}|$) and adaptive threshold ($\bar{\chi}_i$) for $i = 7$, 8, and 9.

switching time and the detected switching time. A detection time delay $\tilde{t} = 9$ s is observed in this case.

Based on Fig. 5 and Fig. 6, we observe that the first six residuals are insensitive to the construction mode switching. These residuals could be used for detecting sensor faults.

The behavior of the residual and the adaptive threshold highly depend on the disturbances ω_1, and the measurement noise ω_2 (related to the accuracy of the sensor) and the selection of the eigenvalues λ. The proposed decision logic guarantees that there will be no false alarms, i.e., there will be no case that the detection system infers the transition to mode 1 although mode 2 is active. However, the delay between the

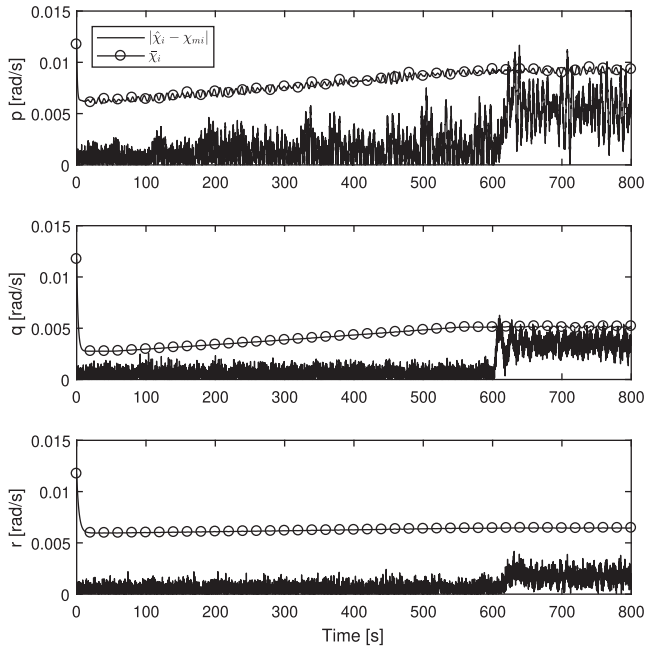

Fig. 8. Residual ($|\hat{\chi}_i - \chi_{mi}|$) and adaptive threshold ($\bar{\chi}_i$) for $i = 10$, 11, and 12.

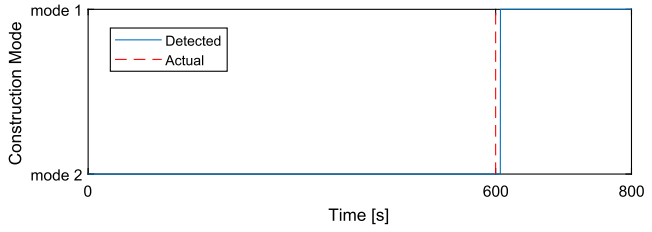

Fig. 9. Mode switch and detected mode switch.

time of detection and the time of the actual transition may be large, or we may miss the detection if the bounds on the disturbances are overestimated or the design parameters of the observer are not optimized.

The adaptive threshold mainly depends on the measurement noise bound (see (33)-(44)). The sensitivity of the proposed detection system with respect to the bound of the measurement noise can be evaluated through the detection delay time. For the sensitivity analysis, we have simulated the adaptive thresholds given in (30), (32)-(45), using an overestimated bound $\bar{\omega}_2'$. The detection delay with respect to the ratio $\frac{\bar{\omega}_{2j}'}{\bar{\omega}_{2j}}$, $\forall\, j \in \{1, \cdots, 12\}$, where $\bar{\omega}_2'$ denotes the overestimated upper bound for the measurement noise, and $\bar{\omega}_2$ denotes the actual bound in (50). With a more conservative setting for the measurement noise, the detection time increases.

As observed from Fig. 10, the detection speed of the designed system decreases as the upper bound of the measurement noise used in the adaptive threshold calculation increases. The selection of the eigenvalues λ can be realized by applying optimization techniques, which are out of the scope of this work.

5. Concluding remarks

In this paper, a novel monitoring system to detect the construction modes during offshore heavy lift constructions is designed to enhance autonomy level and safety during such operations. The proposed detection method is designed following a model based approach, where the magnitude of observer-based residuals are compared to adaptive thresholds. When at least one residual exceeds the corresponding adaptive threshold, the switching of the construction mode is inferred. The adaptive threshold is calculated at every time step based on the observer gains using the measurements of the vessel position, vessel velocity, the tension in the crane wires, and the bounds on the environmental disturbances and measurement noise.

Taking into account the interconnection dynamics, the proposed mode detection system is designed independent of the characteristics of the load and wires, and provides a limited number of residuals and adaptive thresholds to be calculated online. The adaptive thresholds guarantee a more accurate decision making comparing to a fixed threshold. One can easily adapt the proposed monitoring system on vessels with one setting, and needs not to tune the parameters for each offshore heavy lift assignment with a different heavy load.

The proposed monitoring system can be used for the heavy lift vessels to assist the decision making of the human operators, or to obtain decisions without the need of human operators. The fast and reliable decision making plays a key role during the switching of construction mode, where the DP system has to be reconfigured on time to ensure the position stability of the vessel in order to avoid the collision with the platform.

Future work will involve the integration of the construction mode

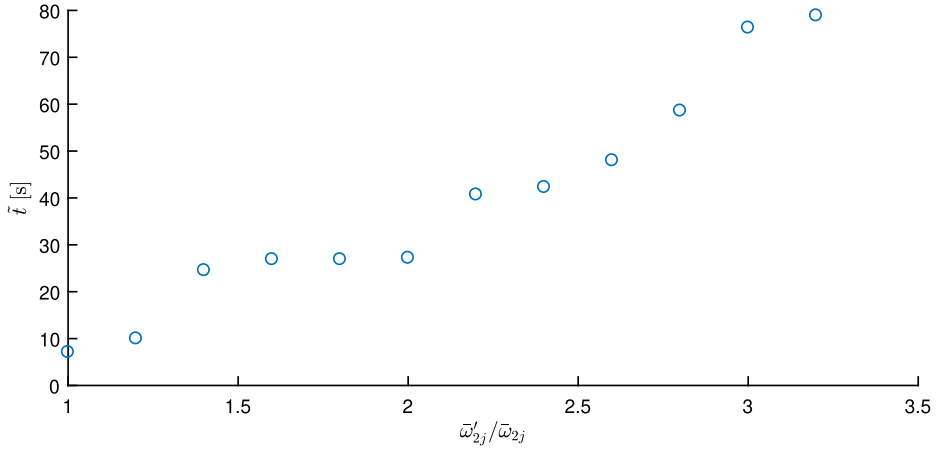

Fig. 10. Detection time delay under different measurement setting of $\bar{\omega}_2$.

monitoring system and the DP system. The performance of the integrated system will be analyzed with respect to high environmental disturbances and measurement noise.

Acknowledgments

This work is financially supported by the program of China Scholarships Council (CSC) with project No. 201607720003.

Appendix A. Calculation of adaptive threshold

Let's consider the following denationalization of the matrix $\mathbf{A}-\mathbf{K}$, we can assume

$$\mathbf{A}-\mathbf{K}=\lambda, \tag{A.1}$$

where $\lambda \in \mathbb{R}^{12\times 12}$ is the diagonal matrix $\lambda = dia\{\lambda_1,\cdots,\lambda_{12}\}$ with elements of eigenvalues of the Hurwitz matrix $\mathbf{AK}$.

Based on (A.1), (26) can then be expressed as:

$$\dot{\widetilde{\chi}} = \lambda\widetilde{\chi} + \widetilde{\gamma} + \widetilde{h} + \omega_1 - (\mathbf{A}-\lambda)\omega_2. \tag{A.2}$$

Solution of the equation above is:

$$\widetilde{\chi} = e^{\lambda t}\widetilde{\chi}(0) + \int_0^t e^{\lambda(t-\tau)}[\widetilde{\gamma} + \widetilde{h} + \omega_1 - (\mathbf{A}-\lambda)\omega_2]d\tau \tag{A.3}$$

$$= e^{\lambda t}\widetilde{\chi}(0) + \int_0^t e^{\lambda(t-\tau)}[\omega_1 - (\mathbf{A}-\lambda)\omega_2]d\tau + \int_0^t e^{\lambda(t-\tau)}(\widetilde{\gamma} + \widetilde{h})d\tau \tag{A.4}$$

where $\widetilde{\gamma}(t) = \gamma(\chi, \mathbf{u}) - \gamma(\chi_m, \mathbf{u})$, and $\widetilde{h}(t) = h(\chi, \mathbf{u}, \zeta, \mathbf{u}_\zeta) - h(\chi_m, \mathbf{u}, \zeta, \mathbf{u}_\zeta)$.

Based on (A.4), $\widetilde{\chi}$ satisfies

$$|\widetilde{\chi}| \leqslant e^{\lambda t}|\widetilde{\chi}(0)| + e^{\lambda t}\int_0^t e^{-\lambda\tau}d\tau(\bar{\omega}_1 + |\mathbf{K}|\bar{\omega}_2)d\tau + \int_0^t e^{\lambda(t-\tau)}(\bar{\gamma} + \bar{h})d\tau \tag{A.5}$$

The last term of (A.5) is the output of a stable first order filter $\mathbf{H}(s)$ with input $\bar{\gamma} + \bar{h}$, with

$$\mathbf{H}(s) = diag\{H_1(s) \;\; H_2(s) \;\; \cdots \;\; H_{12}(s)\}, \tag{A.6}$$

where $H_j(s) = \frac{1}{s-\lambda_j}$, for $j = 1, 2, \ldots, 12$.

Appendix B. Calculation of $\bar{\gamma}$

From (14), we can get

$$\gamma(\chi, \mathbf{u}) - \gamma(\chi_m, \mathbf{u}) = \begin{bmatrix} \mathbf{R}(\eta)\nu - \mathbf{R}(\eta_m)\nu_m \\ \mathbf{M}^{-1}[-\mathbf{C}(\nu)\nu - (-\mathbf{C}(\nu_m)\nu_m)] \end{bmatrix}. \tag{B.1}$$

In(B.1),

$$\begin{aligned} &\mathbf{R}(\eta)\nu - \mathbf{R}(\eta_m)\nu_m \\ &= \mathbf{R}(\eta)\nu - \mathbf{R}(\eta)\nu_m + \mathbf{R}(\eta)\nu_m - \mathbf{R}(\eta_m)\nu_m \\ &= \mathbf{R}(\eta)\omega_\nu + (\mathbf{R}(\eta) - \mathbf{R}(\eta_m))\nu_m, \end{aligned} \tag{B.2}$$

where

$$|\mathbf{R}(\eta)\omega_\nu| \leqslant [||\bar{\omega}_\nu^{1-3}||[1,1,1], ||\bar{\omega}_\nu^{4-6}||[1,1,1]]^T, \tag{B.3}$$

where $\bar{\omega}_\nu$ is the upper bound of the measurement noise ω_ν.

Assume $(\mathbf{R}(\eta) - \mathbf{R}(\eta_m))\nu_m = [a_{n1}, a_{n2}, a_{n3}, a_{n4}, a_{n5}, a_{n6}]^T$, then we have,

$$\begin{aligned} a_{n1} = (c_\phi c_\theta - c_{\phi_m}c_{\theta_m})u_m + (c_\psi s_\theta s_\phi - s_\psi c_\phi - c_{\psi_m}s_{\theta_m}s_{\phi_m} + s_{\psi_m}c_{\phi_m})v_m \\ + (s_\psi s_\phi + c_\psi c_\phi s_\theta - s_{\psi_m}s_{\phi_m} - c_{\psi_m}c_{\phi_m}s_{\theta_m})w_m, \end{aligned} \tag{B.4}$$

$$\begin{aligned} a_{n2} = (s_\psi c_\theta - s_{\psi_m}c_{\theta_m})u_m + (c_\psi c_\phi + s_\phi s_\theta s_\psi - c_{\psi_m}c_{\phi_m} - s_{\phi_m}s_{\theta_m}s_{\psi_m})v_m \\ + (s_\theta s_\psi c_\phi - c_\psi s_\phi - s_{\theta_m}s_{\psi_m}c_{\phi_m} + c_{\psi_m}s_{\phi_m})w_m, \end{aligned} \tag{B.5}$$

$$a_{n3} = (s_{\theta_m} - s_\theta)u_m + (c_\theta s_\phi - c_{\theta_m}s_{\phi_m})v_m + (c_\theta c_\phi - c_{\theta_m}c_{\phi_m})w_m, \tag{B.6}$$

$$a_{n4} = (s_\phi t_\theta - s_{\phi_m}t_{\theta_m})q_m + (c_\phi t_\theta - c_{\phi_m}t_{\theta_m})r_m, \tag{B.7}$$

$$a_{n5} = (c_\phi - c_{\phi_m})q_m + (s_{\phi_m} - s_\phi)r_m, \tag{B.8}$$

$$a_{n6} = (s_\phi/c_\theta - s_{\phi_m}/c_{\theta_m})q_m + (c_\phi/c_\theta - c_{\phi_m}/c_{\theta_m})r_m, \tag{B.9}$$

where $s_\bullet$, $c_\bullet$ denote $sin(\bullet)$ and respectively.

An example for calculation procedure of the boundary of $c_\phi c_\theta - c_{\phi_m}c_{\theta_m}$ is given below:

$$c_\phi c_\theta - c_{\phi_m}c_{\theta_m} \tag{B.10}$$

$$= \frac{1}{2}(c_{\phi-\theta} + c_{\phi+\theta}) - \frac{1}{2}(c_{\phi_m-\theta_m} + c_{\phi_m+\theta_m}) \tag{B.11}$$

$$= \frac{1}{2}(c_{(\phi_m-\omega_\phi)-(\theta_m-\omega_\theta)} - c_{\phi_m-\theta_m}) + \frac{1}{2}(c_{(\phi_m-\omega_\phi)+(\theta_m-\omega_\theta)} - c_{\phi_m+\theta_m}) \tag{B.12}$$

$$= -s_{\frac{1}{2}(2\phi_m-\omega_\phi-2\theta_m+\omega_\theta)}s_{\frac{1}{2}(\omega_\theta-\omega_\phi)} - s_{\frac{1}{2}(2\phi_m-\omega_\phi+2\theta_m-\omega_\theta)}s_{\frac{1}{2}(-\omega_\phi-\omega_\theta)} \tag{B.13}$$

$$\leqslant \bar{\omega}_\theta + \bar{\omega}_\phi. \tag{B.14}$$

By assuming that the roll, pitch, and yaw angle of the vessel is small under DP controller, the boundary of a_{n1}, a_{n2}, a_{n3}, a_{n4}, a_{n5}, and a_{n6} could be calculated. For $i \in \{1, \cdots, 6\}$, denote $\bar{a}_{ni}$ to be the upper bound of a_{ni}, and assume $|(\mathbf{R}(\boldsymbol{\eta}) - \mathbf{R}(\boldsymbol{\eta}_m))\boldsymbol{\nu}_m| \leqslant |\tilde{\mathbf{R}}\boldsymbol{\nu}_m|$, then,

$$\bar{a}_{n1} = (\bar{\omega}_\theta + \bar{\omega}_\phi)u_m + (\bar{\omega}_\theta + 2\bar{\omega}_\phi + 2\bar{\omega}_\psi)v_m + (\bar{\omega}_\theta + 2\bar{\omega}_\phi + 2\bar{\omega}_\psi)w_m, \tag{B.15}$$

$$\bar{a}_{n2} = (\bar{\omega}_\theta + \bar{\omega}_\psi)u_m + (\bar{\omega}_\theta + 2\bar{\omega}_\phi + 2\bar{\omega}_\psi)v_m + (\bar{\omega}_\theta + 2\bar{\omega}_\phi + 2\bar{\omega}_\psi)w_m, \tag{B.16}$$

$$\bar{a}_{n3} = \bar{\omega}_\theta u_m + (\bar{\omega}_\theta + 2\bar{\omega}_\phi + 2\bar{\omega}_\psi)v_m + (\bar{\omega}_\theta + 2\bar{\omega}_\phi + 2\bar{\omega}_\psi)w_m, \tag{B.17}$$

$$\bar{a}_{n4} = \frac{\bar{\omega}_\phi + 2\bar{\omega}_\theta}{1 - 2\bar{\omega}_\theta}q_m + \frac{\bar{\omega}_\phi + 2\bar{\omega}_\theta}{1 - 2\bar{\omega}_\theta}r_m, \tag{B.18}$$

$$\bar{a}_{n5} = \bar{\omega}_\phi q_m + \bar{\omega}_\phi r_m, \tag{B.19}$$

$$\bar{a}_{n6} = \frac{\bar{\omega}_\phi + \bar{\omega}_\theta}{1 - 2\bar{\omega}_\theta}q_m + \frac{\bar{\omega}_\phi + \bar{\omega}_\theta}{1 - 2\bar{\omega}_\theta}r_m. \tag{B.20}$$

Thus,

$$\tilde{\mathbf{R}}(\bar{\boldsymbol{\omega}}_\eta) = \begin{bmatrix} \bar{\omega}_\theta + \bar{\omega}_\phi & \bar{\omega}_\theta + 2\bar{\omega}_\phi + 2\bar{\omega}_\psi & \bar{\omega}_\theta + 2\bar{\omega}_\phi + 2\bar{\omega}_\psi & 0 & 0 & 0 \\ \bar{\omega}_\theta + \bar{\omega}_\psi & \bar{\omega}_\theta + 2\bar{\omega}_\phi + 2\bar{\omega}_\psi & \bar{\omega}_\theta + 2\bar{\omega}_\phi + 2\bar{\omega}_\psi & 0 & 0 & 0 \\ \bar{\omega}_\theta & \bar{\omega}_\theta + 2\bar{\omega}_\phi + 2\bar{\omega}_\psi & \bar{\omega}_\theta + 2\bar{\omega}_\phi + 2\bar{\omega}_\psi & 0 & 0 & 0 \\ 0 & 0 & 0 & 0 & \frac{\bar{\omega}_\phi + 2\bar{\omega}_\theta}{1 - 2\bar{\omega}_\theta} & \frac{\bar{\omega}_\phi + 2\bar{\omega}_\theta}{1 - 2\bar{\omega}_\theta} \\ 0 & 0 & 0 & 0 & \bar{\omega}_\phi & \bar{\omega}_\phi \\ 0 & 0 & 0 & 0 & \frac{\bar{\omega}_\phi + \bar{\omega}_\theta}{1 - 2\bar{\omega}_\theta} & \frac{\bar{\omega}_\phi + \bar{\omega}_\theta}{1 - 2\bar{\omega}_\theta} \end{bmatrix}. \tag{B.21}$$

The Coriolis term for the vessel which is symmetric around x-z plane is expressed as:

$$\mathbf{C}(\boldsymbol{\nu}) = \begin{bmatrix} 0 & 0 & 0 & mz_g r & mw & -mv \\ 0 & 0 & 0 & -mw & mz_g r & mu \\ 0 & 0 & 0 & -m(z_g p - v) & -m(z_g q + u) & 0 \\ -mz_g r & mw & m(z_g p - v) & 0 & I_z r & -I_y q \\ -mw & -mz_g r & m(z_g q + u) & -I_z r & 0 & I_x p \\ mv & -mu & 0 & I_y q & -I_x p & 0 \end{bmatrix}. \tag{B.22}$$

Assume that $\tilde{\mathbf{C}} = \mathbf{C}(\boldsymbol{\nu})\boldsymbol{\nu} - \mathbf{C}(\boldsymbol{\nu}_m)\boldsymbol{\nu}_m = [c_1, c_2, c_3, c_4, c_5, c_6]^T$, and $|\tilde{\mathbf{C}}| \leqslant \bar{\mathbf{C}} = [\bar{c}_1, \bar{c}_2, \bar{c}_3, \bar{c}_4, \bar{c}_5, \bar{c}_6]^T$, an example of the calculation of $\bar{c}_1$ is given below:

$$c_1 = mz_g(r_m p_m - rp) + m(w_m q_m - wq) - m(v_m r_m - vr) \tag{B.23}$$

$$\begin{aligned} &= -mz_g((r_m - \omega_r)(p_m - \omega_p) - r_m p_m) \\ &\quad - m((w_m - \omega_w)(q_m - \omega_q) - w_m q_m) \\ &\quad + m((v_m - \omega_v)(r_m - \omega_r) - v_m r_m). \end{aligned} \tag{B.24}$$

Thus

$$\begin{aligned} |c_1| \leqslant mz_g(\bar{\omega}_r\bar{\omega}_p + \bar{\omega}_r|p_m| + \bar{\omega}_p|r_m|) + m(\bar{\omega}_w\bar{\omega}_q + \bar{\omega}_w|q_m| + \bar{\omega}_q|w_m|) \\ + m(\bar{\omega}_v\bar{\omega}_r + \bar{\omega}_v|r_m| + \bar{\omega}_r|v_m|) \end{aligned} \tag{B.25}$$

$$= \bar{c}_1. \tag{B.26}$$

For the full Coriolis force term,

$$|\tilde{\mathbf{C}}| = |\mathbf{C}(\boldsymbol{\nu})\boldsymbol{\nu} - \mathbf{C}(\boldsymbol{\nu}_m)\boldsymbol{\nu}_m| \tag{B.27}$$

$$\leqslant \bar{\mathbf{C}}(\bar{\omega}_\nu, \boldsymbol{\nu}_m(t)) \tag{B.28}$$

$$= \bar{\mathbf{C}}_1(\bar{\omega}_\nu) + \bar{\mathbf{C}}_2(\bar{\omega}_\nu)\boldsymbol{\nu}_m(t) \tag{B.29}$$

$$= \begin{bmatrix} m(\bar{\omega}_w\bar{\omega}_q + \bar{\omega}_v\bar{\omega}_r + z_g\bar{\omega}_q\bar{\omega}_r) \\ m(\bar{\omega}_w\bar{\omega}_p + \bar{\omega}_u\bar{\omega}_r + z_g\bar{\omega}_p\bar{\omega}_r) \\ m(\bar{\omega}_v\bar{\omega}_p + \bar{\omega}_u\bar{\omega}_q + 2z_g\bar{\omega}_p\bar{\omega}_q) \\ (I_z + I_y)\bar{\omega}_r\bar{\omega}_q + mz_g(\bar{\omega}_u\bar{\omega}_r + \bar{\omega}_w\bar{\omega}_p) \\ (I_z + I_x)\bar{\omega}_p\bar{\omega}_r + mz_g\bar{\omega}_r\bar{\omega}_v \\ (I_x + I_y)\bar{\omega}_p\bar{\omega}_q \end{bmatrix} \tag{B.30}$$

$$+\begin{bmatrix} 0 & m\bar{\omega}_r & m\bar{\omega}_q & 0 \\ m\bar{\omega}_r & 0 & m\bar{\omega}_p & m(\bar{\omega}_w + z_g\bar{\omega}_r) \\ m\bar{\omega}_q & m\bar{\omega}_p & 0 & m(\bar{\omega}_v + z_g\bar{\omega}_q) \\ mz_g\bar{\omega}_r & 0 & mz_g\bar{\omega}_p & mz_g\bar{\omega}_w \\ 0 & mz_g\bar{\omega}_r & 0 & (I_x + I_z)\bar{\omega}_r \\ 0 & 0 & 0 & (I_x + I_y)\bar{\omega}_q \end{bmatrix} \tag{B.31}$$

$$\begin{bmatrix} m(\bar{\omega}_w + z_g\bar{\omega}_r) & m(\bar{\omega}_v + z_g\bar{\omega}_q) \\ 0 & m(\bar{\omega}_u + z_g\bar{\omega}_p) \\ m(\bar{\omega}_u + z_g\bar{\omega}_p) & 0 \\ (I_y + I_z)\bar{\omega}_r & (I_y + I_z)\bar{\omega}_q + mz_g\bar{\omega}_u \\ 0 & (I_x + I_z)\bar{\omega}_p + mz_g\bar{\omega}_v \\ (I_x + I_y)\bar{\omega}_p & 0 \end{bmatrix} \begin{bmatrix} |u_m| \\ |v_m| \\ |w_m| \\ |p_m| \\ |q_m| \\ |r_m| \end{bmatrix}. \tag{B.32}$$

Thus the threshold for the nonlinear term can be expressed as:

$$\bar{\gamma}(\bar{\omega}_2, \chi_m) = \begin{bmatrix} \bar{\omega}_v + |\bar{\mathbf{R}}\boldsymbol{\nu}_m| \\ \mathbf{M}^{-1}\bar{\mathbf{C}} \end{bmatrix}. \tag{B.33}$$

Appendix C. Calculation of $\bar{h}$

For the interconnected term,

$$\begin{aligned} |h(\chi, \mathbf{u}, \zeta, \mathbf{u}_\zeta) - h(\chi_m, \mathbf{u}, \zeta, \mathbf{u}_\zeta)| &= \left|\begin{bmatrix} \mathbf{0} \\ \mathbf{M}^{-1}\tau_1 \end{bmatrix} - \begin{bmatrix} \mathbf{0} \\ \mathbf{M}^{-1}\hat{\tau}_1 \end{bmatrix}\right| \\ &= \begin{bmatrix} \mathbf{0} \\ \mathbf{M}^{-1}|\tilde{\tau}_1| \end{bmatrix} \leqslant \bar{h}(\bar{\omega}_2, \chi_m). \end{aligned}$$

To calculate the threshold $\bar{h}$, the threshold of $\tilde{\tau}$ is analyzed.

$$\tilde{\tau}_1 = \tau_1 - \hat{\tau}_1 \tag{C.1}$$

$$\begin{aligned} &= \begin{bmatrix} \frac{F_{\text{hoist}}}{\|\mathbf{R}_3^T(\eta)(\eta_1 - \eta_3) - \mathbf{p}_{\text{ct}}\|}(\mathbf{R}_3^T(\eta)(\eta_1 - \eta_3) - \mathbf{p}_{\text{ct}}) \\ \frac{F_{\text{hoist}}}{\|\mathbf{R}_3^T(\eta)(\eta_1 - \eta_3) - \mathbf{p}_{\text{ct}}\|}\mathbf{r}_{\text{ct}} \times (\mathbf{R}_3^T(\eta)(\eta_1 - \eta_3) - \mathbf{p}_{\text{ct}}) \end{bmatrix} \\ &- \begin{bmatrix} \frac{F_{\text{hoist}}}{\|\mathbf{R}_3^T(\eta_m)(\eta_1 - \eta_{3m}) - \mathbf{p}_{\text{ct}}\|}(\mathbf{R}_3^T(\eta_m)(\eta_1 - \eta_{3m}) - \mathbf{p}_{\text{ct}}) \\ \frac{F_{\text{hoist}}}{\|\mathbf{R}_3^T(\eta_m)(\eta_1 - \eta_{3m}) - \mathbf{p}_{\text{ct}}\|}\mathbf{r}_{\text{ct}} \times (\mathbf{R}_3^T(\eta_m)(\eta_1 - \eta_{3m}) - \mathbf{p}_{\text{ct}}) \end{bmatrix}. \end{aligned} \tag{C.2}$$

We have

$$\frac{\mathbf{R}_3^T(\eta)(\eta_1 - \eta_3) - \mathbf{p}_{\text{ct}}}{\|\mathbf{R}_3^T(\eta)(\eta_1 - \eta_3) - \mathbf{p}_{\text{ct}}\|} = \frac{\mathbf{R}_3^T(\eta)(\eta_1 - \eta_3) - \mathbf{p}_{\text{ct}}}{\|(\eta_1 - \eta_3) - \mathbf{R}_3(\eta)\mathbf{p}_{\text{ct}}\|}. \tag{C.3}$$

The denominator in (C.4) satisfies

$$\|(\eta_1 - \eta_3) - \mathbf{R}_3(\eta)\mathbf{p}_{\text{ct}}\| \tag{C.4}$$

$$= \|(\eta_1 - \eta_{3m}) - \mathbf{R}_3(\eta_m)\mathbf{p}_{\text{ct}} + (\eta_{3m} - \eta_3) + (\mathbf{R}_3(\eta_m) - \mathbf{R}_3(\eta))\mathbf{p}_{\text{ct}}\|,$$
$$\geqslant \|\|(\eta_1 - \eta_{3m}) - \mathbf{R}_3(\eta_m)\mathbf{p}_{\text{ct}}\| - \|\bar{\omega}_{3\eta}\| - \|\bar{\mathbf{R}}_3\mathbf{p}_{\text{ct}}\|\|, \tag{C.5}$$

where $\bar{\omega}_{3\eta} = [\bar{\omega}_x, \bar{\omega}_y, \bar{\omega}_z]^T$.

The numerator in (C.4) satisfies

$$\begin{aligned} &|\mathbf{R}_3^T(\eta)(\eta_1 - \eta_3) - \mathbf{p}_{\text{ct}}| \\ &= |\mathbf{R}_3^T(\eta_m)(\eta_1 - \eta_{3m}) - \mathbf{p}_{\text{ct}} + (\mathbf{R}_3^T(\eta_m)\eta_{3m} - \mathbf{R}_3^T(\eta)\eta_3) \\ &\quad + (\mathbf{R}_3^T(\eta) - \mathbf{R}_3^T(\eta_m))\eta_1|, \end{aligned} \tag{C.6}$$

$$\leqslant |\mathbf{R}_3^T(\eta_m)(\eta_1 - \eta_{3m}) - \mathbf{p}_{\text{ct}}| + |\bar{\mathbf{R}}_3^T\eta_1| + \|\bar{\omega}_{3\eta}\|[1, 1, 1]^T + |\bar{\mathbf{R}}_3^T\eta_m|. \tag{C.7}$$

Thus, assume

$$\bar{h} = \begin{bmatrix} \mathbf{0} \\ \mathbf{M}^{-1}\begin{bmatrix} F_{\text{hoist}}\bar{\boldsymbol{\beta}} \\ \mathbf{r}_{ct} \times F_{\text{hoist}}\bar{\boldsymbol{\beta}} \end{bmatrix} \end{bmatrix}, \tag{C.8}$$

with

$$\bar{\boldsymbol{\beta}} = \frac{|\mathbf{R}_3^T(\eta_m)(\eta_1 - \eta_{3m}) - \mathbf{p}_{\text{ct}}| + |\bar{\mathbf{R}}_3^T\eta_1| + \|\bar{\omega}_{3\eta}\|\,[1,1,1]^T + |\bar{\mathbf{R}}_3^T\eta_m|}{\|\,(\eta_1 - \eta_{3m}) - \mathbf{R}_3(\eta_m)\mathbf{p}_{\text{ct}}\,\| - \|\,\bar{\omega}_{3\eta}\,\| - \|\,\bar{\mathbf{R}}_3\mathbf{p}_{\text{ct}}\,\|} - \frac{\mathbf{R}_3^T(\eta_m)(\eta_1 - \eta_{3m}) - \mathbf{p}_{\text{ct}}}{\|\,\mathbf{R}_3^T(\eta_m)(\eta_1 - \eta_{3m}) - \mathbf{p}_{\text{ct}}\,\|}. \tag{C.9}$$

References

Badihi, H., Zhang, Y., Hong, H., 2017. Fault-tolerant cooperative control in an offshore wind farm using model-free and model-based fault detection and diagnosis approaches. Appl. Energy 201, 284–307.

Bakker, F., 2015. A conceptual solution to instable dynamic positioning during offshore heavy lift operations using computer simulation techniques. Master's thesis. Delft University of Technology, the Netherlands.

Blanke, M., Kinnaert, M., Lunze, J., Staroswiecki, M., 2016. Diagnosis and fault-tolerant control. Springer-Verlag, Berlin Heidelberg.

Chen, J., Patton, R.J., 1999. Robust Model-based Fault Diagnosis for Dynamic Systems. Kluwer Academic Publishers.

Cho, S., Gao, Z., Moan, T., 2018. Model-based fault detection, fault isolation and fault-tolerant control of a blade pitch system in floating wind turbines. Renew. Energy 120, 306–321.

De Angelo, C.H., Bossio, G.R., Giaccone, S.J., Valla, M.I., Solsona, J.A., Garcia, G.O., 2009. Online model-based stator-fault detection and identification in induction motors. IEEE Trans. Industr. Electron. 56 (11), 4671–4680. https://doi.org/10.1109/TIE.2009.2012468.

de Jong, R., 2018. 3DP: A control system model for combined DP station keeping and active roll reduction.

E. Echavarria, T. Tomiyama, H. Huberts, G. Van Bussel, Fault diagnosis system for an offshore wind turbine using qualitative physics, in: Proc. EWEC, Citeseer, 2008.

Flint, R.J., Stephens, R., 2008. Dynamic positioning for heavy lift aplications. In: Dynamic Positioning Conference, Maritime Technology Society, 2008.

Fonteyn, H., 2015. Stability of the DP system of a crane vessel.

Fossen, T.I., 2011. Handbook of marine craft hydrodynamics and motion control. John Wiley & Sons.

Fu, Q., Wan, H., Qiu, F., 2010. Pipeline leak detection based on fiber optic early-warning system. Proc. Eng. 7, 88–93.

Gao, Z., Cecati, C., Ding, S.X., 2015. A survey of fault diagnosis and fault-tolerant techniques—part i: Fault diagnosis with model-based and signal-based approaches. IEEE Trans. Industr. Electron. 62 (6), 3757–3767. https://doi.org/10.1109/TIE.2015.2417501.

Ghorpade, A., Pereira, F.C., Zhao, F., Zegras, C., Ben-Akiva, M., 2015. An integrated stop-mode detection algorithm for real world smartphone-based travel survey. In: Transportation Research Board 94th Annual Meeting, no. 15–6021, 2015.

Harmsen, E., van Dijk, R., Stuberg, P., 2018. DP-stability during heavy lift operations using a modified kalman filter. In: International Conference on Offshore Mechanics and Arctic Engineering, Vol. 51203, American Society of Mechanical Engineers, 2018, p. V001T01A065.

Hendrapati, M., Sumardi, J., Judhariksawan, Napang, M., Anshar, Subhandi, H., Kristianto, Y., 2017. Offshore installation removal in the interest of navigation safety from international law point of view, vol. 66, pp. 194–204.

Hou, R., Xia, Y., Zhou, X., 2018. Structural damage detection based on l1 regularization using natural frequencies and mode shapes. Struct. Control Health Monitor. 25 (3), e2107.

Isermann, R., 2006. Fault-Diagnosis Systems: An Introduction from Fault Detection to Fault Tolerance. Springer Verlag.

Jenssen, N.A., 2008. On the use of safety moorings in DP operations. In: Dynamic Positioning Conference, 2008.

Khan, F.I., Amyotte, P.R., DiMattia, D.G., 2006. Hepi: A new tool for human error probability calculation for offshore operation. Saf. Sci. 44 (4), 313–334.

Lari, Z.A., Golroo, A., 2015. Automated transportation mode detection using smart phone applications via machine learning: Case study mega city of Tehran. In: Proceedings of the Transportation Research Board 94th Annual Meeting, Washington, DC, USA, 2015, pp. 11–15.

Li, R., Hansen, K., Beltrami, F., et al., 2016. A technical investigation on the ongoing evolution of the market of offshore installation vessels. In: SPE Annual Technical Conference and Exhibition, Society of Petroleum Engineers.

Li, S., Wang, H., Aitouche, A., Tian, Y., Christov, N., 2017. Robust unknown input observer design for state estimation and fault detection using linear parameter varying model. In: Journal of Physics: Conference Series, Vol. 783, IOP Publishing, 2017, p. 012001.

Lloyd's Register, Design code for unmanned marine systems. https://www.cdinfo.lr.org/information/documents/ShipRight/Design%20and%20Construction/Additional%20Design%20Procedures/Design%20Code%20for%20Unmanned%20Marine%20Systems/Design%20Code%20for%20Unmanned%20Marine%20Systems,%20February%202017.pdf (2017).

McKenna, P.R., Leithead, W.E., 2007. Semi-autonomous control of offshore cranes. In: 2007 Institution of Engineering and Technology Conference on Autonomous Systems, pp. 1–6.

Messineo, S., Serrani, A., 2009. Offshore crane control based on adaptive external models. Automatica 45 (11), 2546–2556. https://doi.org/10.1016/j.automatica.2009.07.032.

Mishra, N., Saraf, A., et al., 2019. Leak detection system applicability for offshore and onshore oil and gas pipelines, in: SPE Oil and Gas India Conference and Exhibition, Society of Petroleum Engineers, 2019.

Natarajan, S., Srinivasan, R., 2010. Multi-model based process condition monitoring of offshore oil and gas production process. Chem. Eng. Res. Des. 88 (5), 572–591. https://doi.org/10.1016/j.cherd.2009.10.013. http://www.sciencedirect.com/science/article/pii/S0263876209002780.

Qian, Y., Fang, Y., Lu, B., 2017. Adaptive repetitive learning control for an offshore boom crane. Automatica 82, 21–28. https://doi.org/10.1016/j.automatica.2017.04.003.

Reppa, V., Polycarpou, M.M., Panayiotou, C.G., 2015. Decentralized isolation of multiple sensor faults in large-scale interconnected nonlinear systems. IEEE Trans. Autom. Control 60 (6), 1582–1596.

Reppa, V., Polycarpou, M.M., Panayiotou, C.G., 2016. Sensor fault diagnosis. Found. Trends Syst. Control 3 (1–2), 1–248.

Reppa, V., Timotheou, S., Polycarpou, M.M., Panayiotou, C.G., 2017. Optimization of observer design for sensor fault detection of nonlinear systems. In: 2017 IEEE 56th Annual Conference on Decision and Control (CDC). IEEE, pp. 5155–5160.

Reppa, V., Timotheou, S., Polycarpou, M.M., Panayiotou, C.G., 2018. Performance index for optimizing sensor fault detection of a class of nonlinear systems. IFAC-PapersOnLine 51 (24), 1387–1394.

Sandhåland, H., Oltedal, H., Eid, J., 2015. Situation awareness in bridge operations–a study of collisions between attendant vessels and offshore facilities in the north sea. Saf. Sci. 79, 277–285.

Shafique, M., Hato, E., 2016. Travel mode detection with varying smartphone data collection frequencies. Sensors 16 (5), 716.

Shuguang, L., Qian, G., Wenpu, Z., 2014. Research on active heave compensation for offshore crane. In: The 26th Chinese Control and Decision Conference (2014 CCDC), IEEE, 2014, pp. 1768–1772.

Skaare, B., Egeland, O., 2006. Parallel force/position crane control in marine operations. IEEE J. Oceanic Eng. 31 (3), 599–613. https://doi.org/10.1109/JOE.2006.880394.

Sun, X., Huang, D., Wu, G., 2012. The current state of offshore wind energy technology development. Energy 41 (1), 298–312.

Sun, Y., Li, W., Dong, D., Mei, X., Qiang, H., 2015. Dynamics analysis and active control of a floating crane. Tehnicki vjesnik/Technical Gazette, vol. 22, 6.

Tang, J., Wang, Q., 2008. Online fault diagnosis and prevention expert system for dredgers. Expert Syst. Appl. 34 (1), 511–521.

Waals, O., 2010. On the use of main hoist tension measurement for feed forward in DP systems during offshore installations. In: ASME 2010 29th International Conference on Ocean, Offshore and Arctic Engineering, American Society of Mechanical Engineers, 2010, pp. 393–400.

Wu, L., Yang, B., Jing, P., 2016. Travel mode detection based on gps raw data collected by smartphones: a systematic review of the existing methodologies. Information 7 (4), 67.

Ye, J., 2016. Dynamic positioning during heavy lift operations: Using fuzzy control techniques, nonlinear observer and h-infinity method separately to obtain stable DP systems for heavy lift operations.

Ye, J., Godjevac, M., el Amam, E., 2017. Position control of crane vessel during offshore installations: Using adaptive and robust control methods. In: 2017 21st International Conference on System Theory, Control and Computing (ICSTCC). IEEE, pp. 17–22.

Ye, J., Godjevac, M., Baldi, S., Hopman, H., 2019. Joint estimation of vessel position and mooring stiffness during offshore crane operations. Autom. Constr. 101, 218–226.

Ye, J., Roy, S., Godjevac, M., Baldi, S., 2020. A switching control perspective on the offshore construction scenario of heavy-lift vessels. IEEE Trans. Control Syst. Technol.

Zhang, Q., 2008. Basics of hydraulic systems. CRC Press.